SLAC-PUB-13252
arXiv:0805.3346v1[astro-ph]
May 2008

SUBMITTED TO THE ASTROPHYSICAL JOURNAL
Preprint typeset using LaTeX style emulateapj v. 10/09/06

CONNECTING GALAXIES, HALOS, AND STAR FORMATION RATES ACROSS COSMIC TIME

CHARLIE CONROY[1] & RISA H. WECHSLER[2]
[1]Department of Astrophysical Sciences, Princeton University, Princeton, NJ 08544
[2]Kavli Institute for Particle Astrophysics & Cosmology, Physics Department, and Stanford Linear Accelerator Center, Stanford University, Stanford, CA 94305
Submitted to ApJ, 22 May 2008

ABSTRACT

A simple, observationally-motivated model is presented for understanding how halo masses, galaxy stellar masses, and star formation rates are related, and how these relations evolve with time. The relation between halo mass and galaxy stellar mass is determined by matching the observed spatial abundance of galaxies to the expected spatial abundance of halos at multiple epochs — i.e. more massive galaxies are assigned to more massive halos at each epoch. This "abundance matching" technique has been shown previously to reproduce the observed luminosity- and scale-dependence of galaxy clustering over a range of epochs. Halos at different epochs are connected by halo mass accretion histories estimated from *N*-body simulations. The halo–galaxy connection at fixed epochs in conjunction with the connection between halos across time provides a *connection between observed galaxies across time*. With approximations for the impact of merging and accretion on the growth of galaxies, one can then directly infer the star formation histories of galaxies as a function of stellar and *halo* mass. This model is tuned to match both the observed evolution of the stellar mass function and the normalization of the observed star formation rate – stellar mass relation to $z \sim 1$. The data demands, for example, that the star formation rate density is dominated by galaxies with $M_{\rm star} \approx 10^{10.0-10.5} M_{\odot}$ from $0 < z < 1$, and that such galaxies over these epochs reside in halos with $M_{\rm vir} \approx 10^{11.5-12.5} M_{\odot}$. The star formation rate – halo mass relation is approximately Gaussian over the range $0 < z < 1$ with a mildly evolving mean and normalization. This model is then used to shed light on a number of issues, including 1) a clarification of "downsizing", 2) the lack of a sharp characteristic halo mass at which star formation is truncated, and 3) the dominance of star formation over merging to the stellar build-up of galaxies with $M_{\rm star} \lesssim 10^{11} M_{\odot}$ at $z < 1$.

Subject headings: cosmology: theory — dark matter — galaxies: halos — galaxies: formation — large-scale structure of universe

1. INTRODUCTION

A fundamental goal of galaxy formation studies is to understand what processes govern the stellar content and star formation histories of galaxies. A key piece of this puzzle is relating the stellar masses and star formation rates of galaxies to the masses and formation histories of their associated dark matter halos. Ideally, one would like to make this connection by understanding the physical mechanisms responsible for it from first principles. However, even the best current physically-motivated models of galaxy formation rely on significant approximations of unresolved physics. These approaches, based either on semi-analytic modeling (e.g. White & Frenk 1991; Somerville & Primack 1999; Cole et al. 2000; Hatton et al. 2003; Springel et al. 2001; Croton et al. 2006; Bower et al. 2006), or on hydrodynamical simulations (e.g. Cen & Ostriker 1992; Katz et al. 1996; Springel & Hernquist 2003; Kereš et al. 2005) still have trouble reproducing many basic observational results and suffer from serious uncertainties in the physical ingredients of the models. Although substantial progress has been made in these modeling efforts in recent years, star formation histories in these models and simulations are still sensitive to the interactions between a number of relatively unconstrained physical processes.

Recent observations have begun to measure the galaxy stellar mass function (Fontana et al. 2004; Drory et al. 2004; Bundy et al. 2005; Borch et al. 2006; Fontana et al. 2006; Cimatti et al. 2006; Andreon 2006) and the star formation rate (Noeske et al. 2007b; Zheng et al. 2007a) at high redshift, which complements more precise measurements locally (e.g. Cole et al. 2001; Bell et al. 2003; Brinchmann et al. 2004; Panter et al. 2007; Salim et al. 2007; Schiminovich et al. 2007). At the same time, the evolution of dark matter halos, including their abundance (e.g. Warren et al. 2006; Reed et al. 2007), substructures (Kravtsov et al. 2004; Gao et al. 2004; Reed et al. 2005), and merger and accretion histories (e.g. Wechsler et al. 2002), are becoming ever better understood in the context of the ΛCDM paradigm using numerical simulations.

Several methods have recently been developed that take advantage of these advances to connect the observed galaxy population with dark matter halos using more empirical methods. The most popular of these, known as halo occupation models, typically constrain the statistics of how galaxies populate their host halos using galaxy clustering statistics and space densities (e.g. Scoccimarro et al. 2001; Berlind & Weinberg 2002; Bullock et al. 2002; Zehavi et al. 2004). An emerging alternative is to connect galaxies to the underlying dark matter structure directly, under the assumption that the stellar masses or luminosities of the galaxies are tightly connected to the masses or circular velocities of dark matter halos. Throughout, this latter approach will be referred to as halo "abundance matching" because galaxies of a given stellar mass are matched to halos (*including subhalos*, which are halos that orbit within larger halos) of the same number density or abundance. This approach matches the observed stellar mass function by construction, but has no other observational inputs. Such an approach provides an excellent match to a number of galaxy clustering statistics at multiple epochs (Kravtsov et al. 2004; Tasitsiomi et al. 2004; Vale & Ostriker 2004; Conroy et al. 2006; Berrier et al. 2006; Vale & Ostriker 2006; Marín et al. 2008; Tasitsiomi et al. 2008).

Work supported in part by US Department of Energy contract DE-AC02-76SF00515

The idea of abundance matching galaxies with dark matter halos is not new, and it has been applied to associate a variety of objects with halos since the development of the CDM paradigm (e.g. Mo et al. 1996; Mo & Fukugita 1996; Steidel et al. 1998; Wechsler et al. 1998). However, its successful implementation as a predictive tool requires a full accounting of the halo population, including the substructures that host galaxies, as well as a full accounting of the evolution of the abundance of galaxies as a function of their properties. These elements have only been in place quite recently.

Halo occupation models as well as abundance matching models have been used primarily to understand the connection between galaxies and halos at a fixed epoch, but recent work has begun to use these models to investigate the evolutionary history of galaxies, by combining information about the galaxy–halo connection at given epochs with theoretical input on the evolution of dark matter halos (White et al. 2007; Conroy et al. 2007b; Zheng et al. 2007b; Conroy et al. 2008). In this paper we take the basic idea of abundance matching further, and use it to understand the evolution of the stellar content of galaxies. We use a simple, analytic representation of this framework, which connects dark matter halos to galaxies by matching their abundances, to understand the build-up of stellar mass and the implied star formation rate of galaxies as a function of mass. We focus primarily on redshifts less than one, where the observational results are most reliable, but we expect the approach can be applied more widely and to earlier epochs as observational results improve.

A complementary approach has recently been presented by Drory & Alvarez (2008). While we use the measured galaxy stellar mass function to connect galaxies to dark matter halos and infer the stellar mass buildup and star formation rates of galaxies, they used the measured star formation rates as a function of stellar mass, along with the time derivative of the galaxy stellar mass function, to infer the galaxy merger rate.

The elements of our model are described in detail in §2; §3 presents our primary results, including comparisons to observations. We discuss some of the implications of our model in §3 and summarize in §5. Throughout a flat, ΛCDM cosmology is assumed with the following parameters: $(\Omega_m, \Omega_\Lambda, \sigma_8) = (0.24, 0.76, 0.76)$, and $h = 0.7$ where h is the Hubble parameter in units of 100 km s^{-1} Mpc^{-1}. These cosmological parameters are consistent with the 3rd year *WMAP* estimates (Spergel et al. 2007). A Chabrier (2003) initial mass function (IMF) is adopted throughout.

2. THE MODEL

This section describes the details of our model. We start with a brief overview, and then move to a discussion of the halo mass function and galaxy stellar mass functions in §2.2 and 2.3. The method used to assign galaxies to halos is outlined in §2.4, followed by a description of the approach used to connect galaxies and halos across epochs in §2.5. Introducing a simple estimate for the effect of galaxy mergers and accretion in §2.6 then allows us to compute star-formation histories of galaxies, as discussed in §2.7.

2.1. *Overview*

The model described in detail in the following sections is an extension of previous modeling efforts that have been shown to successfully reproduce an array of data from $z \sim 5$ to the present(Kravtsov et al. 2004; Tasitsiomi et al. 2004; Vale & Ostriker 2004; Conroy et al. 2006; Berrier et al. 2006; Vale & Ostriker 2006; Marín et al. 2008). The first step in our approach is to match the observed abundances of galaxies as a function of stellar mass with the expected abundance of dark matter halos. This step effectively assigns the most massive galaxies to the most massive halos monotonically and with no scatter. Since we include dark matter subhalos, which are halos orbiting within larger halos, we automatically include galaxies that would be observationally classified as satellites, although they are sub-dominant by number ($\sim 10-30\%$ of the galaxies are satellites at any epoch). Thanks to parameterizations of both the evolution of the observed galaxy stellar mass function and of the theoretical halo mass function, this connection between galaxies and dark matter halos can be determined continuously from $z \sim 2$ to $z \sim 0$.

The novel feature of our approach, compared to previous work, is the use of average dark matter mass accretion histories to connect the relations between halos and galaxies across time. *N*-body simulations suggest that the average dark matter halo growth is a simple function of its mass (Wechsler et al. 2002); thus, a halo at any given epoch can be connected to its typical descendants at later epochs. With the connection between galaxies and halos determined at each epoch, the connection between halos across time implies an *average connection between galaxies across time*. At this stage the model produces the average stellar mass growth of galaxies as a function of both galaxy and halo mass. Since we use observationally-derived galaxy stellar mass functions as input, the connection is effectively one between observed galaxies at different epochs.

The final step is to differentiate these average stellar mass growth curves to infer the average mass-growth rates of galaxies. The complication here is separating the growth due to star formation from that due to merging/accretion of other stellar systems. We introduce simple estimates of the contribution due to merging that should bracket the possible effects of merging. This model then allows us to determine the average star formation rates of galaxies as a function of their *halo mass* and redshift, which provides a key constraint on galaxy formation models. The following sections describe this framework in further detail.

2.2. *The halo mass function*

We use the cosmology- and redshift-dependent halo mass function given by Warren et al. (2006) and transform their masses to $M_{\rm vir}$ using an NFW (Navarro et al. 1997) density profile with the concentration–mass relation from Bullock et al. (2001), assuming the updated model parameters given by Wechsler et al. (2006). Our definition of the virial radius corresponds to region with density contrast $\Delta_{\rm vir} = 18\pi^2 + 82x - 39x^2$ with respect to the mean matter density, where $x \equiv \Omega(z) - 1$ (Bryan & Norman 1998). At $z = 0$, $\Delta_{\rm vir} = 337$, and at high redshift $\Delta_{\rm vir}$ asymptotes to 180.

The halo mass function provided by Warren et al. (2006) only considers distinct halos, not the substructure within these distinct halos. Substructure as defined herein consists of halos whose centers are within the virial radii of larger halos, denoted subhalos. Distinct halos, in contrast, are those halos whose centers are not within any larger halos.

We assume that the subhalo fraction is described by

$$f_{\rm sub} \equiv \frac{n_{\rm sub}}{n_{\rm tot}} = 0.2 - \frac{0.1}{3} z, \qquad (1)$$

independent of distinct halo mass, which provides a reasonable fit to data from simulations (see e.g., Fig. 1 of Conroy et al. 2006 we don't include the moderate decrease

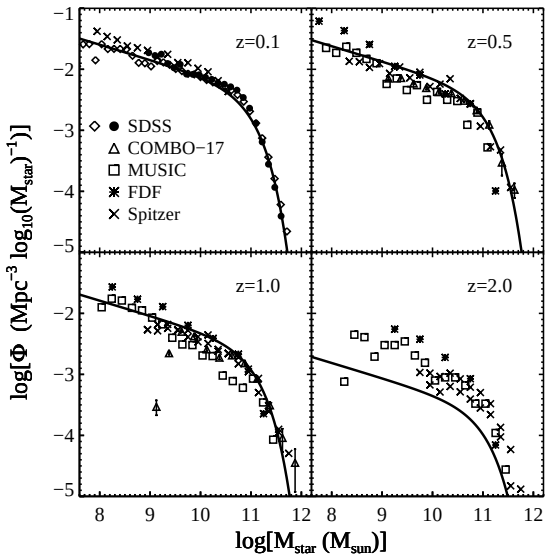

FIG. 1.— Evolution of the galaxy stellar mass function from $z \sim 2$ to $z \sim 0$. Our fiducial model for the evolution of the mass function (*lines*) is compared to the following observational results from the literature: Bell et al. (2003, SDSS; *circles*), Panter et al. (2007, SDSS; *diamonds*) Drory et al. (2005, FDF), Borch et al. (2006, COMBO-17), Pérez-González et al. (2008, *Spitzer)*, and Fontana et al. (2006, MUSIC). The disagreement between model and data at $z = 2$ is discussed in §3.5.

of $f_{\rm sub}$ with increasing mass indicated by simulation data, but this would have a small effect on our results). Note that the subhalo fraction is defined with respect to the mass of the subhalos at the epoch of their accretion. This mass, rather than the present subhalo mass, has been shown to better correlate with observed galaxy properties (Conroy et al. 2006; Berrier et al. 2006). We thus derive an approximate halo mass function that includes both distinct halos and subhalos using this fraction. The results presented below are fairly insensitive to this fraction because it is small; we include it for completeness. Throughout, we refer to both distinct halos and subhalos as halos.

2.3. *The galaxy stellar mass function*

At each redshift, the number density $\phi(M,z)$ of galaxies with stellar mass M_* is assumed to be described by a Schechter function,

$$\phi(M,z) = \phi^*(z)\left(\frac{M}{M^*(z)}\right)^{\alpha^*} \exp\left(-\frac{M}{M^*(z)}\right), \qquad (2)$$

where the free parameters $\phi^*(z)$, $\alpha^*(z)$ and $M^*(z)$ are, in principle, functions of redshift. We take the evolution of $M^*(z)$ to be:

$$\log[M^*(z)/M_\odot] = 10.95 + 0.17\,z - 0.07\,z^2, \qquad (3)$$

which is similar to the form advocated by Fontana et al. (2006). Note that the evolution in M^* implied from the above formula is mild at $z < 2$. Since the constraints on α^* are weak at higher redshift, we assume for simplicity that it does not evolve:

$$\alpha^* = -1.25, \qquad (4)$$

which is consistent within the errors with available data to $z \sim 2$ (Fontana et al. 2006).

The evolution of $\phi^*(z)$ raises a subtle but important issue. Various authors have measured ϕ^* in redshift bins to $z \sim 2$ and then proceeded to fit the observed $\phi^*(z)$ to a function of the form $\phi^*(z) \propto (1+z)^{-\beta}$. However, it is clear that, modulo small evolution in M^* and α^* (and corrections due to stellar mass loss; cf. §2.7), the time-derivative of $\phi^*(z)$ is simply the cosmic star formation rate (SFR) density. The functional form above, for typical adopted values of $\beta = 1-3$, results in an *increasing* SFR density at late times. This is not observed (e.g. Hopkins 2004).

In order to alleviate this tension, we have chosen to constrain the evolution in $\phi^*(z)$ by requiring both that it reproduce the observed evolution in the stellar mass function and that its derivative match the normalization of the observed star formation rate – stellar mass relation to $z \sim 1$. After some experimentation with different functional forms, we adopt the following evolution of ϕ^*:

$$\phi^*(z) = 2 \times 10^{-3}\, e^{-0.5 z^{2.5}}\ {\rm Mpc}^{-3}. \qquad (5)$$

Note that our parameterization is by no means unique. We have simply attempted to match the observed cosmic star formation rate density implied by our model and the observed stellar mass functions by adjusting the form of $\phi^*(z)$. This functional form is similar to that given in Wilkins et al. (2008) who proposed $\phi^*(z) = 2.5 \times 10^{-3} e^{-0.68 z^{1.2}}$ Mpc^{-3} as the best-fit to a variety of stellar mass function data.

The zero-points of the Schechter parameters approximately reproduce the local set of parameters determined by a variety of authors (Cole et al. 2001; Bell et al. 2003; Wang et al. 2006; Panter et al. 2007). Figure 1 compares the evolution of the galaxy stellar mass function in our model to various observational estimates. Our adopted Schechter parameters somewhat overpredict the abundance of low-mass galaxies at $z = 0.5$ and underpredict the abundances of all galaxies at $z = 2$. The latter disagreement is discussed in §3.5.

There is a second, perhaps more serious, tension created by comparison of the evolution of the stellar mass function and the global SFR density. At $z \gtrsim 1$ the integral of the star formation rate density does not equal the stellar mass density (Nagamine et al. 2006; Hopkins & Beacom 2006; Pérez-González et al. 2008; Wilkins et al. 2008). This tension can largely be removed if the IMF evolves with redshift (Davé 2008; Wilkins et al. 2008) because the SFR probes the high-mass end of the IMF while the bulk of the stellar mass is contained in low-mass stars. An evolving IMF at $z \gtrsim 1$ is also suggested by recent work on the evolution of the mass-to-light ratio of elliptical galaxies (van Dokkum 2008) and the abundance patterns of metal-poor stars (Lucatello et al. 2005; Tumlinson 2007a,b). Whether this is the ultimate solution, or whether the solution lies in a more mundane systematic error in one of the measured quantities is not currently clear. Because of this tension at high redshift, we focus our analysis below $z \sim 1$, where the cosmic SFR density and stellar mass density are consistent with each other assuming a non-evolving IMF.

2.4. *Abundance matching: from halos to galaxies*

We assume that every galaxy resides in a dark matter halo and that there is a tight connection between the stellar mass of a galaxy and the mass of its associated dark matter halo. In the limit of zero scatter between galaxy and halo mass, halos of a given mass can be connected to galaxies of a given stellar mass by matching their abundances directly:

$$n_g(> M_{{\rm star},i}) = n_h(> M_{{\rm vir},i}), \qquad (6)$$

where n_g and n_h are the galaxy and halo mass functions, respectively (note that the halo mass function here includes both distinct halos and subhalos). In effect, this prescription assigns the most massive galaxies to the most massive halos monotonically. Since more massive halos are more strongly clustered at all epochs, this mapping implies that more massive/more luminous galaxies will also be more strongly clustered than less massive/less luminous ones, in qualitative agreement with a variety of clustering measurements (e.g. Zehavi et al. 2005; Coil et al. 2006; Li et al. 2006; Meneux et al. 2008). This simple approach is surprisingly successful at quantitatively matching an array of observations at multiple epochs and scales including mass-to-light ratios, clustering measurements, and close pair counts (Kravtsov et al. 2004; Tasitsiomi et al. 2004; Vale & Ostriker 2004, 2006; Berrier et al. 2006; Conroy et al. 2006; Marín et al. 2008), confirming that it can be used with confidence herein.

2.5. *Mass accretion histories: from halo growth to galaxy growth*

Analysis of cosmological N-body simulations has shown that halo mass growth can be described by a simple functional form (Wechsler et al. 2002):

$$M_{\rm vir}(a) = M_0 \exp\left[-2a_c\left(\frac{a_0}{a}-1\right)\right], \quad (7)$$

where $a = (1+z)^{-1}$, M_0 is the mass of the halo at the redshift of observation a_0, and a_c is the average formation scale factor of the halo, the single free parameter in the functional form defined above. Following Wechsler et al. (2002), we adopt the following parameterization of a_c, which provides a good fit to N-body simulations:

$$a_c(M_{\rm vir}) = \frac{4.1}{c(M_{\rm vir})(1+z)}. \quad (8)$$

where $c(M_{\rm vir})$ is the halo concentration– halo mass relation at $z = 0$. We use the model given by Bullock et al. (2001) and the updated parameters provided in Wechsler et al. (2006) for $c(M_{\rm vir})$.

In the previous section we showed how to construct $M_{\rm star} - M_{\rm vir}$ relations as a function of redshift. The relation between a halo of mass $M_{\rm vir}$ at one epoch and its mass at some latter epoch is known via Equation 7. This relation between halos across time allows us to connect the $M_{\rm star} - M_{\rm vir}$ relations across time and hence allows us to determine the stellar growth of galaxies.

For example, we can start with a halo mass $M_{\rm vir}$ at some early epoch. The $M_{\rm star} - M_{\rm vir}$ relation at that epoch then determines the stellar content of the halo. We can then evolve this halo to a later epoch via Equation 7. With the $M_{\rm star} - M_{\rm vir}$ relation at this later epoch we can then read off the stellar content of the halo at this later epoch. Continuing this process allows us to build up the full stellar mass growth of the galaxy sitting at the center of this evolving halo. This process can be repeated for all halos of all masses, allowing one to determine the stellar mass growth of galaxies as a function of dark matter halo mass.

Equation 7 does not apply to subhalos and yet we have included subhalos in our analysis up to this point. There are at least two reasons why this issue will not significantly impact our results. First, at any given epoch the majority of subhalos were only recently accreted (Gao et al. 2004; Zentner et al. 2005), and thus Equation 7 should provide a reasonable approximation to the mass growth history of subhalos over most of their evolution. Second, as mentioned above, subhalos constitute a small fraction of the total halo population ($\sim 10-30\%$ at any epoch) and thus this approximate treatment should have a small effect on our conclusions.

2.6. *The impact of merging on galactic growth*

Galaxies can grow in stellar mass by either star formation or by the cannibalism of smaller galaxies (e.g. Ostriker & Hausman 1977). Both processes can in general contribute to the average stellar mass growth of galaxies. We are interested primarily in the inferred star formation rates as a function of redshift, stellar mass, and halo mass, and we thus seek a simple way of accounting for the impact of galaxy merging on the stellar mass growth of galaxies. In what follows we present an estimate for the accretion rate of smaller galaxies onto the halos of larger galaxies. We then consider two assumptions for the fates of these accreted systems that will bracket the range of possibilities. In the first, we allow all of the stellar material accreted onto the halo to rapidly merge with the central galaxy, thereby increasing the mass of the central galaxy. The other possibility we consider is that the accreted material remains within the host halo of the central galaxy but does not add to its measured luminosity. In other words, the accreted material either remains as bound satellite galaxies or ends up as diffuse stellar material not detected in standard survey photometry. In this latter scenario stellar mass growth is thus determined entirely by star formation. These two scenarios are referred to as the "merger" and "no-merger" scenarios below. We now describe the merger scenario in more detail.

Halos grow via the accretion of smaller halos. The mass spectrum of accreted halos is approximately self-similar in $m' = m/M_z$ where m and M_z are the mass of the accreted halo and mass of the parent halo at redshift z (Lacey & Cole 1993; Stewart et al. 2007). The spectrum can be approximated as:

$$\frac{{\rm d}f}{{\rm dln}m'} = \frac{\sqrt{m'}}{2.6}\exp\left[-\left(\frac{m'}{0.7}\right)^6\right], \quad (9)$$

where f is the fraction of mass accreted in clumps of mass m'. The exponential cut-off is steep because $m' > 1$ is not allowed by definition. Equation 9 is a fit to the simulation results of Stewart et al. (2007). This function does not integrate to unity, indicating that a significant fraction, $\sim 30-50\%$, of the parent mass is accreted in a diffuse component of dark matter (Stewart et al. 2007). Whether or not this component is truly diffuse or is in clumps of very small mass (e.g. Madau et al. 2008) is immaterial for our purposes, because in either case this component will not bring in additional stars.

With the mass accretion spectrum in hand, the halo growth rate, $\dot{m}_{\rm halo}$, can be converted into a stellar growth rate due to mergers, $\dot{m}_{\rm stars}$, via:

$$\dot{m}_{\rm stars} = \dot{m}_{\rm halo}\int \frac{{\rm d}f}{{\rm dln}m'}\frac{M_{\rm star}}{M_{\rm vir}}(M_{\rm vir},z){\rm dln}m', \quad (10)$$

where $\frac{M_{\rm star}}{M_{\rm vir}}(M_{\rm vir},z)$ is the redshift- and halo mass-dependent stellar-to-halo mass ratio determined in §2.4. Equation 10 can be thought of as a convolution of the halo mass accretion spectrum with the relations between halo mass and stellar mass determined in previous sections. In other words, Equation 9 tells us the types of halos that are accreted, and §2.4 tells us the stellar content of these accreted halos. In the following

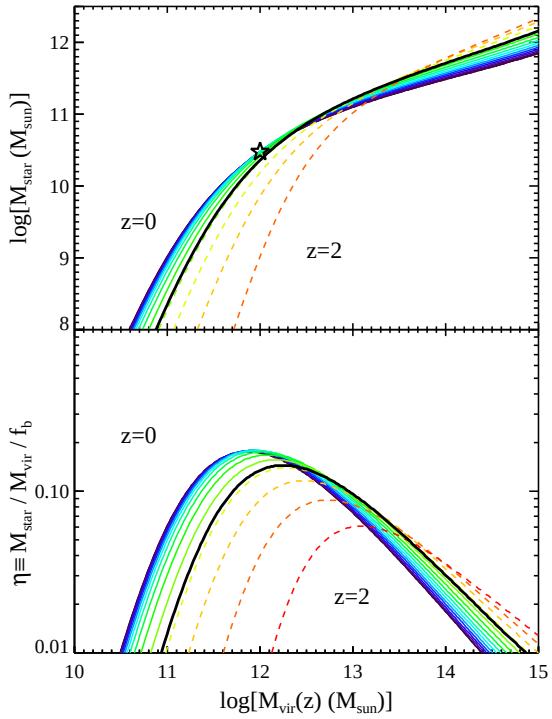

FIG. 2.— *Top Panel:* The relation between galaxy stellar mass and halo mass from $z = 2$ to $z = 0$, using the abundance matching model. *Bottom Panel:* Fraction of available baryons that have turned into stars (integrated star formation efficiency) as a function of the halo mass and redshift, where f_b is the universal baryon fraction. The star marks the location of the Milky Way at $z = 0$. The thick black line represents the relation at $z = 1$. The relations at $z > 1$ (*dashed lines*) should be treated with caution; see §3.5 for details.

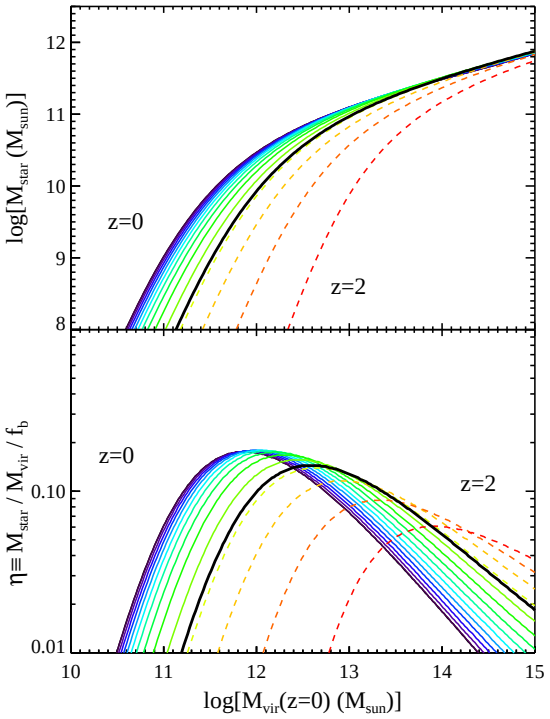

FIG. 3.— *Top Panel:* The redshift-dependent relation between galaxy stellar mass and the mass of the halo to which it will belong at $z = 0$. By focusing on a fixed $z = 0$ halo mass, one can read up in the plot from $z = 2$ to $z = 0$ to infer the stellar mass growth of an average galaxy that, by $z = 0$, resides in that halo. *Bottom Panel:* Fraction of available baryons that have turned into stars as a function of the $z = 0$ halo mass. The thick black line represents the relation at $z = 1$. The relations at $z > 1$ (*dashed lines*) should be treated with caution; see §3.5 for details.

sections we will present results for both the merger and no-merger scenarios, and in §4.3 we discuss how our results bear on the relative importance of merging and star formation on the stellar growth of galaxies.

2.7. *From galactic growth to star-formation rates*

With an estimate for the amount of stellar mass growth that is due to merging/accretion, the SFR of an average galaxy can then be estimated straightforwardly via a derivative of the portion of stellar mass growth attributed to star formation. The relation between mass growth and star formation is complicated by mass loss due to dying stars. We take into account this effect with the following formula:

$$f_{\rm loss}(t) = 5 \times 10^{-2} \ln\left(\frac{t + 3 \times 10^5}{3 \times 10^5}\right), \qquad (11)$$

where t is in years and $f_{\rm loss}(t)$ is the fraction of mass lost by time t for a co-eval set of stars. This formula is a fit to the mass loss of simple stellar populations with a Chabrier (2003) IMF (Renzini & Ciotti 1993; Bruzual & Charlot 2003). Note that only $\sim 60\%$ of the stellar mass formed in a burst of star formation remains after several gigayears, and that the stellar mass remaining includes stellar remnants. With the full stellar mass growth curve one can then iteratively solve for the star formation rate required to generate such growth given the above mass-loss rate formula.

3. MODEL IMPLICATIONS

The previous section presented a method for connecting the stellar masses and star formation rates of galaxies to dark matter halos over a range of epochs. This section explores these relations and compares to observations where possible.

3.1. *Halo-galaxy connections*

Implementing the abundance matching technique discussed in §2.4 at various epochs yields the relations between halo and galaxy mass shown in the top panel of Figure 2. The generic shape of the relation is governed simply by the Schechter-like functions of both the galaxy stellar MF and the halo MF. The redshift outputs are spaced equally in $(1+z)^{-1}$. One novel conclusion drawn from this figure is that, since $z \sim 2$, the stellar mass of galaxies residing in halos of mass $\sim 10^{12.5} M_\odot$ stays roughly constant, at $\sim 10^{11} M_\odot$. Over the redshift range considered, above this mass scale, halo growth out-paces stellar mass growth, while below this scale, galaxy growth is more vigorous than halo growth.

The relation shown in Figure 2 applies to central galaxies and to satellites where the halo mass refers to the mass at the time of accretion onto their host (see, e.g. Conroy et al. 2006, for a discussion). Although the assumption of zero scatter is idealized, several recent works indicate that this scatter is small, with ~ 0.15 dex of scatter in galaxy luminosity at fixed mass (Zheng et al. 2007b; van den Bosch et al. 2007; Hansen et al. 2007; Wechsler et al. 2008). Including this level of scatter does not substantially impact the mean relation shown in this plot. As a comparative reference, we show the location of the Milky Way in this figure, as determined from the halo mass estimates of Klypin et al. (2002). The Milky Way falls directly on our mean relation.

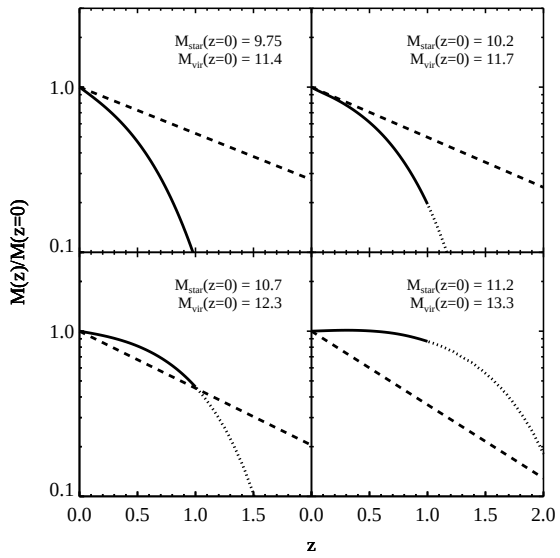

FIG. 4.— Fraction of mass assembled as a function of redshift. Each panel compares the fraction of a galaxy's stellar mass that is assembled (*solid and dotted lines*) to the fraction of the galaxy's parent halo mass that is assembled (*dashed lines*). The stellar growth curves are dotted at $z > 1$ to indicate that this regime should be treated with caution; see §3.5 for details. The four panels display the assembly history for a range of galaxies with $z = 0$ stellar and halo masses shown in the legend, in units of $\log(M_\odot)$. It is clear that, at lower mass, a larger fraction of the halo is in place at early times compared to higher mass. The opposite trend is true for stellar masses.

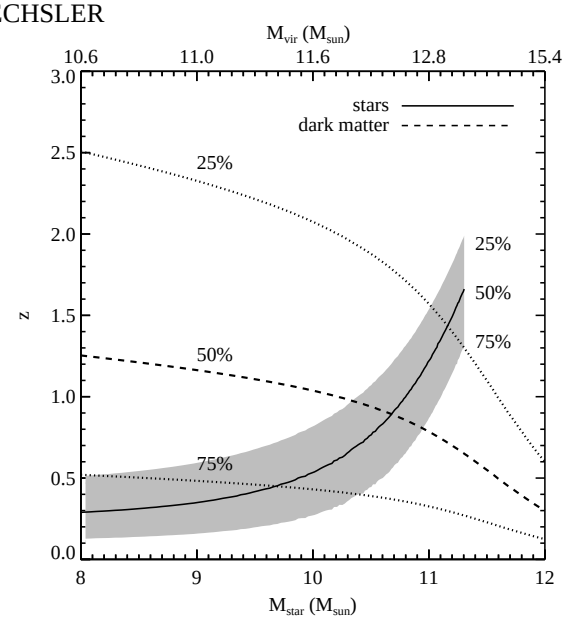

FIG. 5.— Average formation times for galaxies (*solid line and shaded region*) and halos (*dashed and dotted lines*) as a function of $z = 0$ galaxy and halo mass. Lines and shaded region indicate the redshift at which 25%, 50%, and 75% of the final mass was assembled, as labeled in the figure. For example, a galaxy with stellar mass $10^{10} M_\odot$ at $z = 0$ assembled 50% of its final mass by $z \approx 0.5$. Such a galaxy resides in a halo of mass $10^{11.6} M_\odot$, which was half assembled by $z \approx 1.0$. At $M_{\rm star} \lesssim 10^{10.7} M_\odot$ halos are assembled before galaxies while at higher masses the opposite is true, in agreement with the trends seen in Figure 4.

The shape and mild evolution of the $M_{\rm star} - M_{\rm vir}$ relation shown in Figure 2 provides a clear interpretation of the observed relation between stellar and halo mass from $z \sim 1$ to $z \sim 0$ reported in Conroy et al. (2007c). These authors used the dynamics of satellite galaxies orbiting around brighter host galaxies to constrain halo masses, and found that in bins of galaxy stellar mass, halo mass evolves little or not at all since $z \sim 1$ below $M_{\rm star} < 10^{11} M_\odot$ but increases by a factor of several above this stellar mass. This qualitative trend is evident in Figure 2, and can be attributed to the fact that above $M_{\rm star} \sim 10^{11} M_\odot$ the relation shallows, implying that a small shift in the relation over time produces a large change in the halo mass of a given galaxy mass over time.

We define the integrated efficiency of star formation as $\eta \equiv M_{\rm star}/M_{\rm vir}/f_b$, where $f_b = 0.17$ is the universal baryon fraction (Spergel et al. 2007). This efficiency quantifies the fraction of available baryons that have been converted into stars, and peaks where integrated star formation is most efficient. Abundance matching readily predicts $\eta(M_{\rm vir})$ and is shown as a function of redshift in the bottom panel of Figure 2. The first thing to note is that this result implies that the overall efficiency of converting baryons into stars is quite low, never reaching more than $\sim 20\%$ of the potentially available baryons. Although perhaps somewhat surprising, note also that the global stellar mass density is $\sim$4–8 times less than the global baryon density. This low efficiency is also in good agreement with current estimates for the total and stellar mass of the Milky Way (Klypin et al. 2002), with estimates of halo masses from weak lensing measurements combined with stellar mass estimates (Mandelbaum et al. 2006), with halo occupation models both at $z \sim 0$ and $z \sim 1$ (Zheng et al. 2007b), and with inferences from a joint analysis of the stellar mass function and the mass—metallicity relation (Baldry et al. 2008).

Two important trends are apparent. First, the location of the peak decreases to lower halo masses with time. The latter trend is a manifestation of at least one meaning of "downsizing" (Cowie et al. 1996), and is a natural implication of the fact that the characteristic stellar mass evolves more slowly than the characteristic halo mass (see §4.1 for a discussion of downsizing). Second, the amplitude of the peak star-formation efficiency increases with decreasing redshift, although the magnitude of this trend is somewhat uncertain. This is due to the rather uncertain evolution of ϕ^*, which directly affects the evolution of the peak of $\eta(M_{\rm vir})$; varying the evolution in ϕ^* over a reasonable range changes the amount of evolution in the peak by less than a factor of two. More accurate observational constraints on $\phi^*(z)$ are required to more robustly pin down the evolution in $\eta(M_{\rm vir})$. However, the trend that the peak shifts to lower masses with time is robust to uncertainties in $\phi^*(z)$. The mass at which baryons are most efficiently converted into stars shifts by about a factor of ~ 20 from $z = 2$ to $z = 0$, from $M_{\rm vir} \sim 10^{13} M_\odot$ to $M_{\rm vir} \sim 10^{11.7} M_\odot$.

These trends, including the factor of ~ 2 increase in peak efficiency from $z \sim 1$ to $z \sim 0$, and the mild decrease in halo mass at which the peak occurs, agree well with halo occupation modeling of galaxies at these epochs (Zheng et al. 2007b).

As discussed in §2.5, we know from *N*-body simulations the full mass growth histories of dark matter halos statistically for a given cosmology. These accretion histories allow us to evolve a halo of mass $M_{\rm vir}(z)$ at redshift z forward in time to the mass such a halo will have by $z = 0$, $M_{\rm vir}(z = 0)$. We can couple these halo accretion histories to the $M_{\rm star} - M_{\rm vir}$ relations discussed above to determine the relation between a halo's mass at $z = 0$ and the stellar mass content of that halo as a function of redshift.

The resulting relations are shown in the top panel of Figure 3. The $z = 0$ halo mass can be thought of as a unique tag for each (average) galaxy. A vertical slice through Figure 3 thus traces out the trajectory of an average galaxy at different redshifts. From this plot one can thus read off *directly* the average stellar mass build-up of galaxies as a function of their $z = 0$ halo mass. These relations are uniquely determined by the relations between galaxies and halos at fixed epochs in conjunction with the evolution of halos demanded by our fiducial cosmology.

A clear and robust inference from this figure is that the stellar mass of galaxies residing in $z = 0$ halos of mass $\gtrsim 10^{14} M_\odot$ was mostly assembled by $z \sim 2$. This agrees qualitatively with the modest evolution in the massive end of the observed galaxy stellar mass function since $z \sim 2$ (e.g. Fontana et al. 2004; Drory et al. 2004; Bundy et al. 2005; Borch et al. 2006; Fontana et al. 2006; Cimatti et al. 2006; Andreon 2006; Brown et al. 2007, 2008; Pérez-González et al. 2008; Cool et al. 2008). Note however that the input to our model is the observed galaxy stellar mass function, so for example if observations do not account for the low surface brightness intracluster light associated with central galaxies in massive halos (e.g. Gonzalez et al. 2005; Zibetti et al. 2005; Krick & Bernstein 2007), then our model will also fail to incorporate this component. The diffuse light could contain as much mass as the central galaxy, and should thus be taken into account when modeling massive galaxies (see discussion in Monaco et al. 2006; Conroy et al. 2007b,a; Purcell et al. 2007). Here however our focus is on stellar growth and star formation in more modestly-sized halos.

The bottom panel of Figure 3 shows the integrated star formation efficiency of galaxies at various epochs as a function of their $z = 0$ halo mass. For halo masses less than $\sim 10^{12} M_\odot$ the integrated efficiency is a monotonically increasing function of time. At higher masses the efficiency rises, peaks, and then falls with increasing time, and at masses greater than $\sim 10^{14} M_\odot$ the integrated efficiency is a continually decreasing function of time since $z = 2$.

3.1.1. *Galaxy growth versus halo growth*

A perhaps more revealing illustration of the results in Figure 3 are shown in Figure 4. There the stellar mass growth of a galaxy is compared to the growth of its parent dark matter halo for four representative $z = 0$ stellar masses. For stellar masses $\lesssim 10^{10.7} M_\odot$ (corresponding to $M_{\rm vir} \lesssim 10^{12.3} M_\odot$), fractional halo growth since $z = 2$ is much more mild than stellar growth. This low-mass regime can thus be thought of as 'internally-dominated', where growth is not controlled by extra-halo processes. Stellar growth in this regime is thus driven by gas physics related to cooling, star formation, and feedback.

The situation is qualitatively different at higher masses. At stellar masses $\gtrsim 10^{11} M_\odot$ (corresponding to $M_{\rm vir} \gtrsim 10^{13} M_\odot$), fractional halo growth is much stronger than stellar growth at $z < 2$. This is not surprising in light of the fact that the massive end of the stellar mass function appears to be approximately in place since $z \sim 1$ (Fontana et al. 2004; Drory et al. 2004; Bundy et al. 2005; Borch et al. 2006; Fontana et al. 2006; Cimatti et al. 2006; Wake et al. 2006; Brown et al. 2007; Cool et al. 2008). This high-mass regime is thus 'externally-dominated', in contrast to lower-mass systems. High-mass systems are primarily accreting copious amounts of dark matter, some fraction of which will bring in bound stellar systems (e.g. satellite galaxies). The system — defined loosely as the region within the halo virial radius — is thus growing in a larger sense, while the galaxy at the center of the halo is not. This figure does not include the potentially massive component of stellar light associated with a diffuse background, known as the intracluster light. For a discussion of the importance of this component see Conroy et al. (2007b) and references therein.

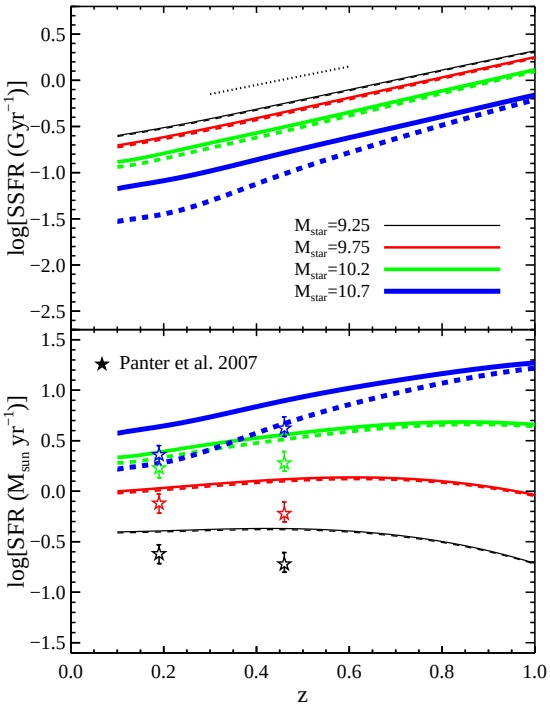

FIG. 6.— *Top Panel:* Average specific star formation rate history as a function of redshift, for galaxies with $z = 0$ stellar masses given in the legend (in units of $\log(M_\odot)$). The dotted line indicates a slope of unity. *Bottom Panel:* Star formation rate history as a function of redshift for the same model galaxies. The solid and dashed lines represent our model for two prescriptions to relate stellar growth to star formation. The solid lines are for the no-merger model while the dashed lines are for the merger model (see §2.6 for details). Observed star formation histories from Panter et al. (2007) for galaxies of the same $z = 0$ stellar masses as the model predictions are included for comparison. For reasons discussed in the text, the model is likely not reliable at $z > 1$. Note that results for both the model and data are *average* relations.

The average formation times for galaxies and halos is shown in Figure 5. Here we plot the redshift at which 25%, 50%, and 75% of the final mass was assembled, for both the stars accreted onto the galaxy and for the dark matter mass accreted onto the halo. Since we are investigating only average properties, recall that in our model each galaxy mass is assigned a unique halo mass, and thus each average galaxy has a unique halo mass and stellar mass, and unique formation times for both of those components. It is clear that the stellar mass in lower mass systems formed later than in high mass systems, while the dark matter halos display the opposite trend. Although this general trend has now been evident from a range of data, this figure ties together the available information on galaxy and halo growth.

3.2. *The star formation history of galaxies*

The star formation rate (SFR) and specific star formation rate (SSFR $\equiv$ SFR/$M_{\rm star}$) for average galaxy trajectories are shown in Figure 6 as a function of redshift for several representative $z = 0$ stellar masses. The SSFR is approximately

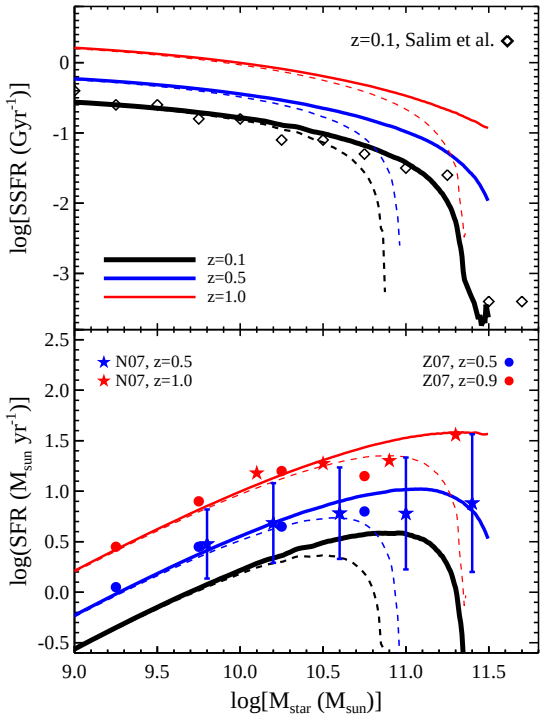

FIG. 7.— SSFR (*top panel*) and SFR (*bottom panel*) as a function of galaxy stellar mass at various epochs. Note that the two panels display equivalent information. Observational results from Noeske et al. (2007b) are included and labeled N07, as are $z \sim 0$ data from Salim et al. (2007) and data from Zheng et al. (2007a), labeled Z07. Error bars denote 1σ scatter, not the error on the mean, and are included for only one set of data for clarity. The solid and dashed lines represent the no-merger and merger models, respectively (see §2.6 for details). The no-merger model is clearly a better match to the data at all epochs. Note that the model describes *average* relations of SFR with mass.

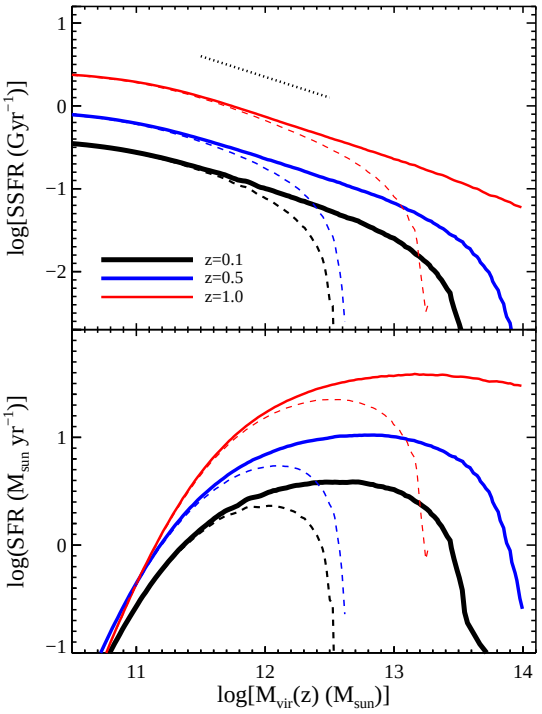

FIG. 8.— SSFR (*top panel*) and SFR (*bottom panel*) as a function of halo mass at various epochs. As in previous figures, the solid and dashed lines represent the no-merger and merger models, respectively (see §2.6 for details). These two assumptions only impact the derived SFR at high masses, and the data favor the no-merger model (see Figure 7). In the top panel the dotted line indicates a slope of –0.5. Note that the model describes *average* relations of SFR with mass.

self-similar in galaxy mass for $z < 1$ and scales with redshift as $\log(\mathrm{SSFR}) \propto z$. Lower mass galaxies have higher specific star formation rates at all times. In this and subsequent figures we include two different treatments for the importance of merging on stellar mass growth. The solid lines represent the assumption that all stellar mass growth is due to star formation in situ, while the dashed lines represent the prescription, described in §2.6, that includes mergers and accretion.

The SSFR for the most massive galaxies ($M_{\rm star} \gtrsim 10^{11}\,M_\odot$) is the least constrained in our model because the massive end of the stellar mass function evolves little at $z < 2$, and so the SFR is a derivative of a nearly constant function. This can be seen in the top panel of Figure 3, where it is clear that small uncertainties/changes in the stellar mass or halo mass scale can cause relatively large uncertainties in the star formation rates. When discussing star-formation rates we restrict ourselves to stellar masses less than $\sim 10^{11}\,M_\odot$ where the conversion between stellar mass growth and SFR is most reliable.

The bottom panel of Figure 6 shows the average SFR of galaxies as a function of $z = 0$ stellar mass. The results in this figure are not directly accessible to observations at high redshift because the observations do not tell us the connection between galaxies at different epochs. Without this information, following the SFH of a particular galaxy across time is not possible with observations of the distant past. However, such information is at least in principle attainable from consideration of the stellar populations of galaxies in the local universe. Attempts at inferring the SFH of galaxies in this way have concluded that the SFR peaked earlier for more massive galaxies, and for galaxies less massive than $\sim 10^{10} M_\odot$ the data are consistent with a constant SFH, at least since $z \sim 1$ (Lee et al. 2007; van Zee 2001; Heavens et al. 2004; Panter et al. 2007). The model results presented in Figure 6 is compared to the results from Panter et al. (2007) who have used the stellar populations of local galaxies to constrain their mass-dependent star formation histories. Our model reproduces the general trends well, though there is a $\sim 0.1-0.2$ dex offset between the model and data.

Furthermore, the trends in Figure 6 shed light on the phenomenon known as 'downsizing' (e.g. Cowie et al. 1996; Brinchmann & Ellis 2000; Juneau et al. 2005) whereby more massive systems formed the bulk of their stars at earlier epochs compared to less massive systems. While it is clear that star formation has peaked earlier in more massive systems, it is also apparent from the figure that at any epoch, more massive galaxies have higher star formation rates and smaller specific star formation rates than less massive galaxies. We discuss this issue further in §4.1.

3.3. *SFR dependence on galaxy and halo mass*

Our model allows us to calculate the SSFR and SFR of galaxies as functions of stellar mass and redshift; these are shown in Figure 7. As above, the figure includes two different prescriptions for relating stellar growth to star formation. One possibility is that all stellar growth is due to star formation (*solid lines*) while the other allows for some fraction of stellar growth to be attributed to merging (*dashed lines*; see

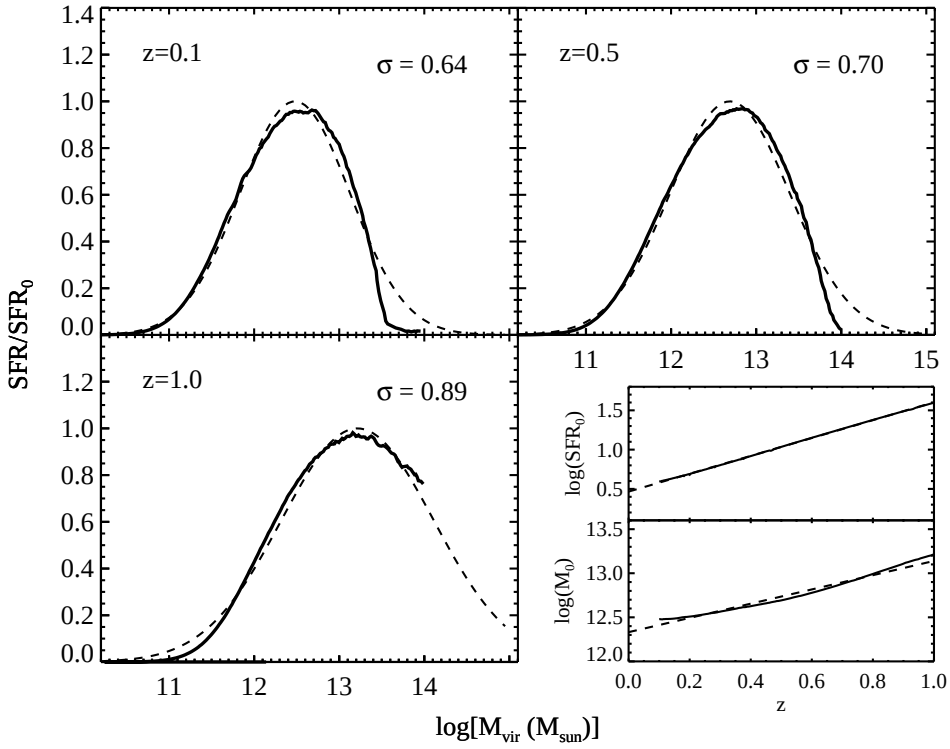

FIG. 9.— SFR as a function of halo mass at various epochs for our preferred, no-merger model (*solid lines*). In this figure we include Gaussian fits to the SFR($M_{\rm vir}$) relations (*dashed lines*). The inset shows the best-fit normalization, $\rm SFR_0$, and mean, M_0, as a function of redshift (*solid lines*), along with linear fits (*dashed lines*) to these relations, which are barely distinguishable from the relations themselves. The dispersion is a weak function of redshift and is thus only included in the three larger panels for clarity— the average dispersion between $0.1 < z < 1.0$ is $\sigma = 0.72$. Note that at higher redshift the turn-over at high masses is not resolved and the fits there should thus be treated with caution.

§2.6).

The model is compared to a variety of data from the literature over the redshift interval $0 < z < 1$. In all cases the data are meant to represent *average* star formation rates as a function of stellar mass (i.e. the average star formation rate of *all* — both red and blue — galaxies at a given stellar mass). The completeness-corrected average SFR–*M*star relation from Noeske et al. (2007b) was constructed based on the completeness corrections of Lin et al. (2008, K. Noeske private communication) in order to account for red galaxies with no detectable levels of star formation. The results from Zheng et al. (2007a) were derived from stacked data and can thus be interpreted as average relations. Finally, the results from Salim et al. (2007) were determined from data with sufficient sensitivity to detect extremely low levels of star formation and can thus also be interpreted as an average relation over all galaxies at a given stellar mass.

It is clear from Figure 7 that the assumption that all stellar growth is due to star formation (i.e. the no-merger scenario; *solid lines*) provides a much better match to the data at stellar masses $\gtrsim 10^{10} M_{\odot}$. For this reason we adopt this assumption as the fiducial model. At lower masses the no-merger and merger scenarios yield the same predictions for the star formation rates (i.e., even with maximal merging, incoming satellite galaxies do not contribute any appreciable stellar mass) The importance of star formation over merging in galactic growth is discussed further in §4.3.

The normalization of the model depends on the evolution of ϕ^*, the redshift-dependent normalization of the stellar mass function, while the shape depends on α^* and M^*, although the latter two dependencies are much weaker than the first. Notice that we have tuned the evolution of ϕ^* to reproduce the normalization of the SFR–$M_{\rm star}$ relations but not the shape of these relations. The shape is thus a robust prediction of our approach, while the normalization agrees with the data by construction.

It is worth mentioning here why the approach taken in this paper is particularly useful. The current generation of hydrodynamic simulations and semi-analytic models are not capable of reproducing the redshift-dependent trends shown in Figure 7 (Davé 2008). The cause of this discrepancy is not currently understood, although Davé (2008) speculates that an evolving IMF can alleviate the tension. Regardless, it is clear that until this tension is resolved, using either hydrodynamic simulations or semi-analytic models to interpret the observations and connect them to the formation and evolution of halos requires caution. Our approach matches the observations by construction and it can thus be used with more confidence for interpreting the data. Its main limitation, and the main advantage of the simulations, is that our model makes no reference to the underlying physical processes governing these relations. However, the connection between observables and halo mass derived from our approach should be very helpful in informing these more physical models.

Figures 6 and 7 can be thought of as consistency checks between the model and data, since many of the implications that can be drawn from these figures are readily available from the data themselves. In contrast, Figure 8 contains a variety of novel results. This figure shows the model predictions for the SFR and SSFR in galaxies *as a function of their host dark*

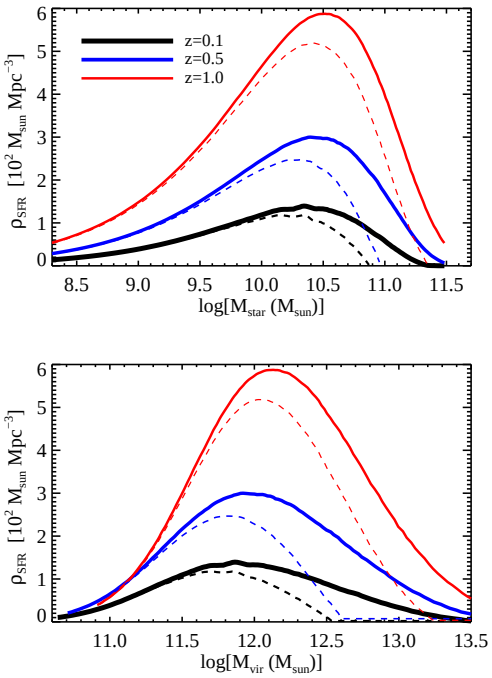

FIG. 10.— *Top Panel:* SFR density as a function of stellar mass and redshift. *Bottom Panel:* SFR density as a function of halo mass and redshift. These plots illustrate the contribution to the global SFR density for galaxies of a given stellar mass (*top panel*) and for galaxies residing in a given halo mass (*bottom panel*). As in previous figures, we include SFR estimates for both the assumption that the stellar growth is entirely due to star formation (*solid lines*), and a simple prescription to account for the amount of stellar growth due to mergers and accretion (*dashed lines*, see §2.6). This figure demonstrates that the bulk of star formation at $z \leq 1$ occurs in relatively massive galaxies and in halos of mass $10^{11.5-12.5} M_\odot$.

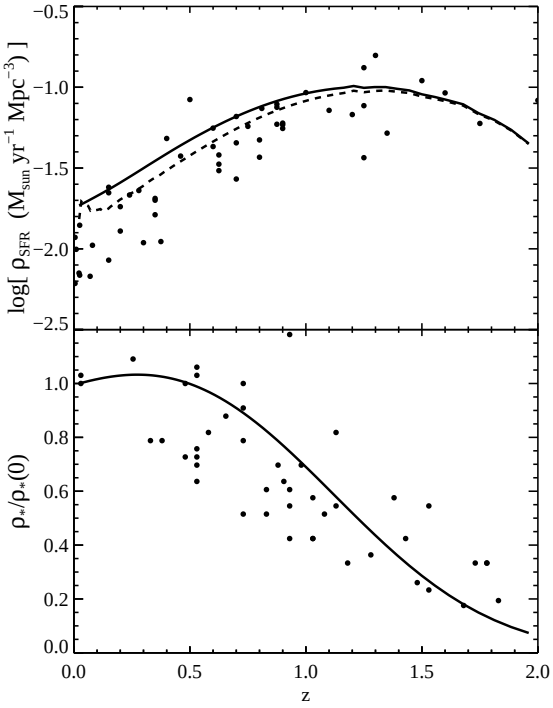

FIG. 11.— *Top Panel*: Cosmic SFR density as a function of redshift. Our model predictions both for the no-merger (*solid line*) and merger (*dashed line*) models are compared to the data compilation of Hopkins (2004, *circles*). *Bottom Panel*: Cosmic stellar mass density as a function of redshift (*solid line*) compared to the data compilation of Wilkins et al. (2008, *circles*).

matter halo masses.

An interesting consequence of Figure 8 is that the halo mass at which the most vigorous star formation occurs is not a strong function of redshift. In addition, the peak in SFR occurs over a large range of halo masses, rather than at one well-defined scale. Moreover, the SSFR–$M_{\rm vir}$ relation appears to be almost scale-free up to $M_{\rm vir} \sim 10^{13} M_\odot$ for our favored model, with the normalization steadily decreasing with time and a non-evolving slope. Over the range $10^{11.0} \lesssim M_{\rm vir} \lesssim 10^{13.0} M_\odot$, the redshift- and mass-dependent relation can be approximated by:

$$\mathrm{SSFR} \approx \left(4.9 + 0.9z\right) M_{\rm vir}^{-0.5}\ \mathrm{Gyr}^{-1}. \qquad (12)$$

The relation between SFR and halo mass shown in Figure 8 can be thought of as the most fundamental of the relations discussed in this work, as this redshift-dependent relation gives rise to all other relations. This relation thus provides a direct link between observations and models in the sense that any model which reproduces the trends in Figure 8 will automatically match the variety of observational results discussed herein. This connection between SFR and halo mass, determined entirely from observations with our simple approach, can thus be of general use to the modeling community in constraining models of cooling, feedback, and star formation in galaxies.

Figure 9 shows the SFR–$M_{\rm vir}$ relations again, now with Gaussian fits (note that the y-axis is shown here in linear units). It is clear that the relations are well-characterized as Gaussian except perhaps at the highest masses at low redshift (where our model is least well-constrained) and at high masses at high redshift where the turn-over is not resolved. The fits in these regimes should thus be treated with caution.

The Gaussian fits are characterized by three parameters: the peak, SFR_0, mean, M_0, and dispersion, σ. The first two parameters are shown as a function of redshift in the inset panels of Figure 9. These parameters are very well approximated with the following linear relations:

$$\log(\mathrm{SFR}_0) = 0.47 + 1.1z \qquad (13)$$

$$\log(M_0) = 12.3 + 0.81z. \qquad (14)$$

These fits are included in the inset panels. The dispersion is a much weaker function of redshift than either the normalization or the mean. The dispersion ranges from 0.64 at $z = 0.1$ to 0.89 at $z = 1.0$ with a mean value of 0.72 over the whole interval $0.1 < z < 1.0$. It is important to recognize that, while the general functional form and redshift-dependent trends are robust predictions of our model, the precise values are subject to uncertainty because the observations themselves, to which the model is tied, still have substantial uncertainties.

In all of these figures it is important to keep in mind that we are presenting *average* relations between various quantities. At first glance Figure 8 might suggest that there would be no red galaxies (where star-formation has ceased) at $z \sim 1$. There can of course be such galaxies, as there can also be galaxies with SFR in excess of the average relation presented in Figure 8.

3.4. *Global properties*

Figure 10 plots the SFR density as a function of stellar mass at $z = 0.1, 0.5$, and 1.0. This quantity is the SFR density con-

tributed by galaxies with mass $M_{\rm star}$ and is produced by multiplying the SFR–$M_{\rm star}$ relation by the galaxy stellar mass function, $\Phi(M_{\rm star})$. This quantity is thus well-constrained by the observational data. In the figure, this quantity is plotted both as a function of the stellar and dark matter halo mass.

In the top panel, the peak for our favored model (*solid lines*) is ~ 0.5 dex lower than the characteristic mass of the stellar mass function, M^*, at all epochs, indicating that the bulk of the SFR density is contributed by galaxies a factor of ~ 3 in mass below M^*. In other words, the characteristic galactic mass in which stars form since $z \lesssim 1$ is a factor of ~ 3 lower than the characteristic galactic mass dominating the mass density.

This peak in the SFR density does not change appreciably from $z \sim 0$ to $z \sim 1$. The bulk of star formation at $z \lesssim 1$ never occurs in small systems, rather it is always dominated by relatively massive, $M_{\rm star} \sim 10^{10.0-10.5} M_\odot$ galaxies. Similarly, the peak as a function of $M_{\rm vir}$ (*bottom panel*) decreases only slightly, by at most ~ 0.5 dex from $z = 1$ to $z = 0$. These results imply that a typical star in the Universe forms in galaxies of similar mass, both in terms of stars and dark matter, from $z \sim 1$ to $z \sim 0$. The principle difference with redshift is that the distribution of masses increases with time, so that stars are more likely to form in a variety of systems at later epochs.

Finally, Figure 11 compares our model predictions for the evolution of the cosmic SFR density and stellar mass density to data compilations provided by Hopkins (2004) and Wilkins et al. (2008), respectively. The top panel includes the model prediction for the SFR under the two different assumptions discussed in §2.6. The agreement between model and data at $z < 1$ in this figure is largely by construction, as mentioned in §2.3, but is included here for completeness. The discrepancy between model and data at $z > 1$, which is more apparent in Figure 1 but is also seen here, is discussed in the next section.

3.5. *The model at $z > 1$*

In this section we have focused largely on redshifts less than one. At higher redshifts the model fails to match the observed cosmic SFR stellar mass density evolution at $z > 1$ as shown in Figure 11, and, relatedly, the normalization of the stellar mass function at $z = 2$, shown in Figure 1. This disagreement arises due to a more generic discrepancy between observed SFR indicators and stellar mass estimates, as discussed in §2.3. As discussed in that section, one possible explanation is that the IMF evolves with redshift (e.g. Wilkins et al. 2008), although we emphasize that this possibility is controversial. Nonetheless, the generic inconsistency between *observations* implies that our model cannot be robustly applied to $z > 1$.

Moreover, it is plausible that our assumption of a tight correlation between stellar mass and halo mass breaks down at higher redshift (cf. discussion in Conroy et al. 2008). This tight correlation is strongly supported at $0 < z < 1$ by the observed stellar mass-dependent autocorrelation function of galaxies, in the sense that more massive galaxies are more strongly clustered (Li et al. 2006; Meneux et al. 2008). This observational result can be most easily explained if more massive galaxies reside in more massive halos because halo clustering strength is a monotonically increasing function of halo mass (e.g. Zehavi et al. 2005; Conroy et al. 2006).

This observational trend has not been unambiguously confirmed at $z > 2$ (Adelberger et al. 2005), except perhaps at the very highest masses (Quadri et al. 2007). It is clear however that there is strong *restframe UV luminosity*-dependent clustering at these early epochs (Adelberger et al. 2005; Lee et al. 2006; Ouchi et al. 2005). By analogy with stellar masses at low redshift, this trend can be understood if UV luminosity, and hence the star formation rate, is strongly and monotonically correlated with dark matter halo mass. If this is the correct interpretation, then our model must be modified at these early epochs (see e.g. Conroy et al. 2008).

3.6. *Dependence on cosmological parameters*

The halo mass functions and halo mass accretion histories in this model are dependent on cosmological parameters. Because it effects the shape and normalization of the mass function, the normalization of the power spectrum can have a large affect on our results. The analytic framework for these halo properties described in §2.2 allows us to straightforwardly explore the effect of cosmological parameters. Here we just consider the effect of the normalization of the power spectrum as specified by the rms fluctuations measured in 8 Mpch^{-1} spheres, σ_8.

We find that the impact of σ_8 on our results is imperceptible for $z = 0$ halo masses less than $\sim 10^{14} M_\odot$. This is due to the fact that the dependence of the halo mass function on σ_8 is much stronger at the massive end. When considering a change from our fiducial model with $\sigma_8 = 0.76$ to a model with $\sigma_8 = 0.90$, even at $M_{\rm vir} = 10^{14} M_\odot$ the difference in halo abundance is < 0.3 dex, and at $M_{\rm vir} = 10^{13} M_\odot$ it is < 0.1 dex. The accretion histories are also a function of σ_8, but again the effect is only manifest at high halo masses. Since the bulk of our results focus on halo masses $\lesssim 10^{14} M_\odot$, we conclude that the uncertainty in σ_8 does not impact our conclusions.

4. DISCUSSION

4.1. *Downsizing: what, when, and where*

The phenomenon known as "downsizing", coined by Cowie et al. (1996), has received much attention recently, and, perhaps confusingly, has been attributed to a number of related but nevertheless different phenomena. In its most general sense the term highlights a shift in a *preferred mass scale* of a phenomenon related to stellar growth or star formation. With an observationally-constrained model for the redshift-dependent connections between star formation, stellar mass, and halo mass, we are in a position to clarify and outline the relations between the various meanings of downsizing. For clarity, we focus discussion on galaxies with $M_{\rm star} < 10^{11} M_\odot$ and $z < 1$, where our results are most reliable (see e.g. Cattaneo et al. 2008, for a theoretical discussion of downsizing for higher mass systems).

Originally, downsizing described the observation that the maximum K-band luminosity of galaxies above a SSFR threshold decreases with time (Cowie et al. 1996). In this definition, the SSFR threshold is independent of redshift. In Figure 7 we can see that a line of constant SSFR will indeed include more massive galaxies at earlier epochs, consistent with this notion. However, inspection of the full relations in this figure shows that this notion of downsizing is driven by the global phenomenon that all galaxies have lower star formation rates at later times. In fact, these relations do not appear to show any preferred scale with stellar mass (except possibly at very high stellar masses), but rather they shift self-similarly in time as noted by Noeske et al. (2007b,a).

Figures 8 and 9 display another type of downsizing in the sense that the dark matter halo mass at which star formation is

most intense shifts to lower masses at later times. This trend is apparent in both our favored model where stellar growth is entirely due to star formation (*solid lines*) and in the model that includes stellar growth due to mergers (*dashed lines*), suggesting that this form of downsizing is a generic feature of dark matter halos. Indeed, Neistein et al. (2006) has argued that downsizing arises naturally from the accretion histories of the dark matter halos themselves. While this is an intriguing possibility, the uncertain relation between halos and galaxies (connected in their terms by the competition between gas heating and cooling), makes their conclusions difficult to interpret at face value.

Downsizing has also been attributed to the observation that more massive galaxies seem to have formed the bulk of their stars earlier. This type of downsizing has been referred to as "archaeological downsizing" because it is observed in the fossil record of the spectra of $z \approx 0$ galaxies. It has been most convincingly demonstrated in local elliptical galaxies where one finds that more massive galaxies formed the bulk of their stars earlier and over shorter timescales than less massive galaxies (Thomas et al. 2005).

This form of downsizing can be seen clearly in Figure 4, which shows that the most massive galaxies formed the bulk of their stars earlier than less massive galaxies. From Figure 6 it is also clear that the peak of the SFR occurs at earlier times for more massive systems. Note however that in the top panel of Figure 6 there is no clear scale in the SSFR except perhaps for the most massive galaxies, and thus there is little evidence for any type of downsizing in this relation.

A final meaning of downsizing concerns the sites where the bulk of stars are being formed at any epoch. This form of downsizing implies that stars are being formed in preferentially smaller systems at later times. In Figure 10 it is clear however that the typical masses hosting the bulk of star formation has not changed appreciably since $z \sim 1$. There is thus no evidence for this form of downsizing given the available data.

It is understandable, in light of the preceding discussion, that the term downsizing has been used to describe so many related but different phenomena, and that some authors find no evidence for a downsizing phenomenon. As we have seen in the various relations between SFR, SSFR, stellar mass, halo mass, and redshift, some show a shift in preferred scales with time, and some do not. Downsizing, of whatever type, thus manifests itself only in certain relations, and not in others.

4.2. *A characteristic halo mass?*

Recently several theoretical studies have raised the possibility of a characteristic halo mass below which star formation occurs, and above which star formation is truncated (Kereš et al. 2005; Dekel & Birnboim 2006; Birnboim et al. 2007; Cattaneo et al. 2007). In this section we focus on the observational evidence for or against a *sharp or narrow range in halo masses* over which galaxy properties, such as star formation rates, change dramatically.

This characteristic mass scale, which is thought to be $M_{\rm vir} \sim 10^{12} M_\odot$ at $z \sim 0$, may be related to the observed stellar mass scale at which many properties of galaxies qualitatively change (e.g. Kauffmann et al. 2003). The fundamental gas dynamical effect occurring in halos above this characteristic scale is thought to be the formation of a stable shock through which infalling gas must cross, thereby raising the temperature of this newly accreted gas to the virial temperature of the halo (Kereš et al. 2005). Accreted gas that is shock-heated is known as 'hot-mode' accretion, while gas that is not shock-heated is referred to as 'cold-mode' accretion.

There are a number of outstanding issues related to any possible sharp transition in e.g. galaxy colors or star formation rates occurring at a characteristic halo mass. First, the transition from cold to hot-mode accretion does not appear to be particularly sharp in hydrodynamic simulations (Kereš et al. 2005). There is clearly a transition region, but it is broad, spanning the mass range $\sim 10^{11-12} M_\odot$. Moreover, the establishment of a hot atmosphere does not guarantee that star formation will cease because such gas will still radiate and can thus cool (although hot, low density gas is more susceptible to further heating processes than cool, dense gas). Indeed, the cooling time of the intracluster medium at the centers of massive clusters is in many cases $< 10^9$ Gyr (Sanderson et al. 2006). One thus must propose additional mechanisms that are capable of supplying sufficient energy to keep the hot atmosphere from cooling and hence forming stars. Possible mechanisms include feedback from active galactic nuclei (e.g. Croton et al. 2006; Cattaneo et al. 2008), heating by dynamical friction (Miller 1986; Khochfar & Ostriker 2007), thermal conduction (Zakamska & Narayan 2003), virialization heating (Wang & Abel 2008), heating by ram-pressure drag (Dekel & Birnboim 2008), and supernovae heating. The relevance of these or other mechanisms to the shut-down of star formation is currently a subject of active debate (see Conroy & Ostriker 2007, for a recent evaluation).

Our results on the relation between star formation rates and halo masses can shed light on this issue. In particular, our model provides a bridge between the observations and the underlying dark matter structure. At stellar masses $\lesssim 10^{11} M_\odot$, where our results are most reliable, we find no significant evidence for a *sharp* characteristic halo mass at which star formation rates dramatically change, when considering average relations between star formation, stellar and halo mass. This statement is based on the following inferences.

The scale at which galaxy properties such as color and morphology appear to change qualitatively is at $M_{\rm star} \sim 10^{10.3} M_\odot$ (Kauffmann et al. 2003). Our abundance matching results shown in Figure 2 demonstrate that this stellar mass corresponds to a halo mass of $\sim 10^{12} M_\odot$ at $z \sim 0$, in qualitative agreement with the characteristic halo mass scale mentioned above (Dekel & Birnboim 2006).

In Figure 8, however, for our favored model (the no merging model) there is no abrupt change in the average star formation rate as a function of halo mass for $M_{\rm vir} \lesssim 10^{13} M_\odot$, at either $z \sim 0$ or at higher redshifts. Instead, over this range the SFR–$M_{\rm vir}$ relation is approximately Gaussian with a broad peak at $M_{\rm vir} \lesssim 10^{12.5} M_\odot$ at $z \sim 0$. We reiterate that the $z \sim 0$ SFR–$M_{\rm vir}$ relation is determined by 1) the $z \sim 0$ SFR–$M_{\rm star}$ relation, where the model and data agree well, and 2) our connection between stellar and halo mass at $z \sim 0$. This latter connection is known to reproduce the observed clustering properties of galaxies (Conroy et al. 2006; Zheng et al. 2007b) and also agrees with weak lensing measurements of halo masses as a function of stellar mass (Mandelbaum et al. 2006). At higher redshifts the peak shifts to higher halo masses, and the gradual roll-over at the high-mass end seen in the $z \sim 0$ average SFR–$M_{\rm vir}$ relation disappears. The data is thus consistent with there being no drop in star formation whatsoever above a given halo mass scale at higher redshifts, at least for halos with mass $M_{\rm vir} \lesssim 10^{13} M_\odot$, where we focus our results. In this figure the merger model does indeed produce a sharp break in the SFR–$M_{\rm vir}$ relation, but recall that this model fails to

reproduce the observed SFR–$M_{\rm star}$ relation shown in Figure 7.

It is important to stress that these conclusions at $z \sim 0$ rest on the reliability of the observed $z \sim 0$ average SFR–$M_{\rm star}$ relation, as reported by Salim et al. (2007) (see also Schiminovich et al. 2007). These authors caution that the star formation rates inferred for massive galaxies, $M_{\rm star} \gtrsim 10^{11.5} M_\odot$, may in some cases be upper limits because low levels of *UV* flux may arise from old stellar populations (e.g. Rich et al. 2005) that are not typically included in modeling of star formation rates. Interpreting low levels of *UV* flux has historically been challenging for this reason. Similar issues arise at higher redshifts. Note however that we do not rely on these massive galaxies for our conclusions because they reside in very massive, $M_{\rm vir} > 10^{14} M_\odot$, halos.

Moreover, as shown in Figure 8, there is clearly no scale in the specific star formation rate as a function of halo mass — it is approximately a power law that scales as SSFR$\propto M_{\rm vir}^{-0.5}$ over at least two orders of magnitude in halo mass. Again, these statements apply to halos with mass $M_{\rm vir} \lesssim 10^{13} M_\odot$. At higher masses our model is not well-calibrated.

In sum, while a well-defined characteristic halo mass, above which star formation is truncated, may be an appealing mechanism for generating red sequence galaxies (Cattaneo et al. 2008), there is no clear indication from our data-driven model that this scale is particularly sharp. It is clear that observed galaxy properties change qualitatively around a stellar mass scale of $M_{\rm star} \sim 10^{10.3} M_\odot$, corresponding in our model to a halo mass of $\sim 10^{12} M_\odot$. We simply emphasize that the data favors a rather gradual shift in galaxy properties across this halo mass scale.

4.3. *The relative importance of star formation and merging to galactic growth*

In order to translate our model predictions for stellar mass growth into predictions for star formation rates, we have to make assumptions for the fraction of mass growth attributed to mergers, as described in §2.6. One approach is to assume that all stellar material accreted onto the halo remains in the halo as satellite galaxies or is stripped and remains in the stellar halo. This is the no-merger model described above. In this model all stellar growth is due to star formation. The second approach is to assume that all of the accreted material immediately falls onto the central galaxy and hence contributes to its stellar growth. These two approaches should bracket the range of possibilities, as in reality some accreted material will lose energy and merge with the central galaxy, while other material will remain as bound satellites, or will merge with the central galaxy yet be dispersed outside the photometric radius.

For galaxies with stellar mass $\lesssim 10^{10} M_\odot$, these two treatments for the importance of merging on stellar growth lead to indistinguishable predictions for the resulting star formation rates (see e.g. Figure 7). Thus, we can state with confidence that galaxies below this mass range grow almost entirely by star formation, at least since $z < 1$ where we focus our analysis. This result can be understood as follows. Halos grow via the accretion of smaller halos. By inspection of the lower panel of Figure 2, it is clear that for halos with mass $\lesssim 10^{11.5} M_\odot$, corresponding to stellar masses $\lesssim 10^{10} M_\odot$, the fraction of available baryons that have been converted into stars drops precipitously. In other words, for these low mass halos, the even smaller mass halos that are contributing to halo growth are almost entirely devoid of stars. Furthermore, low mass halos have largely completed their growth by $z \sim 1$, as discussed in §2.5, and thus any resulting stellar growth since $z \sim 1$ must come from within the halo, i.e. via star formation. These points were also discussed in Purcell et al. (2007) and are qualitatively consistent with current semi-analytic models (Guo & White 2008). They robustly follow from the integrated star formation efficiencies shown in Figure 2.

At larger stellar masses the two treatments yield different predictions for the star formation rates of galaxies. The results presented in §3.3 show that the data on the SFR–$M_{\rm star}$ relation match the approach that attributes all stellar growth to star formation, at least for stellar masses $\lesssim 10^{11} M_\odot$ and $z < 1$, where we focus our analysis. It thus appears that over this entire stellar mass and redshift range, stellar mass growth in galaxies is dominated by star formation. These conclusions are largely consistent with results from cosmological hydrodynamic simulations and may help explain the dominance of disk galaxies at these stellar masses, if disks are a signpost of a relatively quiescent history (Maller et al. 2006).

At first glance this may seem surprising because at these higher masses one expects accretion of halos massive enough to host large galaxies. The accretion of such objects is, as mentioned above, a generic prediction of *N*-body simulations coupled to our connection between galaxies and halos. Of course, the accretion of stellar material onto the halo need not necessarily lead to growth of the galaxy residing at the center of the halo because the accreted material may either remain in orbit within the halo or may be tidally disrupted before it can spiral into the center. In the latter case, the material will contribute to the observed diffuse intracluster light that is ubiquitous in large dark matter halos (Gonzalez et al. 2005; Zibetti et al. 2005). Indeed, our results indicate that some combination of these two scenarios is precisely what is happening (see also discussion in Conroy et al. 2007b). Evidence for the former scenario, whereby accreted material remains as bound satellites, is corroborated by the observed increase since $z \sim 1$ in the fraction of galaxies at a given halo mass that are satellites (Zheng et al. 2007b).

In sum, our results suggest that stellar growth since $z \sim 1$ is dominated by star formation, as opposed to mergers, for stellar masses $\lesssim 10^{11} M_\odot$. This conclusion is not readily available from any single observation; rather it emerges upon synthesis of an array of observational data in the context of a framework for relating these observational data to the underlying dark matter structure.

5. SUMMARY

This paper presents a model for the evolution of galaxies that is based on the observationally-motivated assumption of a tight correlation between galaxy stellar mass and dark matter halo mass. This assumption is used to populate halos with galaxies from $z = 2$ to $z = 0$ using theoretical halo mass functions and observationally-constrained galaxy stellar mass functions. Halos (and the galaxies within them) are evolved forward in time using estimates for halo growth calibrated against *N*-body simulations. This then provides the average stellar mass growth of galaxies as a function of $z = 0$ stellar and halo mass. At $M_{\rm star} \lesssim 10^{10} M_\odot$ the model robustly predicts that the vast majority of stellar growth is due to in situ star formation since small halos do not accrete significant amounts of stellar material. At higher masses, where the *halo* merger rate is higher, mergers and accretion could in principle contribute to stellar growth. However, the model agrees with an array of data when all stellar growth at these higher masses

is attributed to star formation (rather than some fraction being due to mergers) for galaxies with $M_{\rm star} \lesssim 10^{11} M_\odot$ at $z < 1$. Our model does not explicitly address the growth history of more massive galaxies.

With the assumption of a one-to-one correlation between stellar and halo mass, the only freedom within our framework is the particular form adopted for the redshift-dependent stellar mass function. We have adopted a form that provides the best fit to a variety of data including the observed stellar mass function at $0 < z < 1$, the cosmic SFR and stellar mass density, and the SFR–$M_{\rm star}$ relation over the range $0 < z < 1$. This model can thus be thought of, in part, as a self-consistent synthesis of the available data relating galaxy SFRs and stellar masses across time; it allows us to connect galaxy populations at a given epoch with those at another epoch. The model also effectively connects the observations to the underlying dark matter structure, thereby providing a bridge between observational results and theoretical work aimed at understanding such observations.

The principle new result that can be obtained from this framework is a directly-constrained form of the star formation rate in galaxies as a function of halo mass. Our approach provides a direct link between observations and these models in the sense that any model which reproduces this constrained relation for SFR($M_{\rm vir}, z$) will automatically match the wide variety of observational results discussed herein, over the last half of the Universe's age. This result can thus help to distinguish between the processes responsible for triggering and halting star formation, and can be directly employed in constraining models and simulations of the physics of galaxy formation.

The success of this simple model at describing an array of data over the stellar mass range $10^9 < M_{\rm star} < 10^{11} M_\odot$ and redshift range $0 < z < 1$ indicates that the relation between galaxies and halos is surprisingly simple, smooth, and monotonic over these ranges. The most significant short-coming of this model is its inability (in its present form) to predict distributions of properties, rather than averages, as a function of stellar and halo mass. Such information is clearly needed to understand the color bi-modality seen in the color-magnitude diagram, as well as the detailed properties of satellite galaxies, and we will address this in future work.

This model relies on observational inputs that are rather uncertain, such as the evolution of the stellar mass function and the IMF, and the quantitative predictions of this model are thus necessarily uncertain. Despite these unavoidable uncertainties, the general trends predicted by this model, such as the dependence of the SFR of galaxies on galaxy and halo mass, are robust and highlight the underlying connections both between the panoply of observations at high and low redshift, and between the observations as a whole and the underlying dark matter distribution.

We thank Andrew Hopkins, Kai Noeske, Ben Panter, Pablo Pérez-González, Samir Salim, and Stephen Wilkins for providing their data in electronic format and substantial help in its interpretation, and Kyle Stewart for providing his simulation results. We thank Marcelo Alvarez, Peter Behroozi, Niv Drory, Sandy Faber, Andrew Hopkins, Andrey Kravtsov, Kai Noeske, and Aristotle Socrates for helpful conversations, and Brian Gerke, Ari Maller, Samir Salim, and David Schiminovich for helpful comments on an earlier draft. CC thanks Jeremy Tinker for generously providing his mass function and cosmology code. RHW thanks the San Francisco skyline for inspiration; CC thanks Princeton for being monotonic. RHW was supported in part by the U.S. Department of Energy under contract number DE-AC02-76SF00515 and by a Terman Fellowship at Stanford University. We thank the Aspen Center for Physics (partially funded by NSF-0602228) for hosting us while much of this work was completed.

REFERENCES

Adelberger, K. L., Steidel, C. C., Pettini, M., Shapley, A. E., Reddy, N. A., & Erb, D. K. 2005, ApJ, 619, 697
Andreon, S. 2006, A&A, 448, 447
Baldry, I. K., Glazebrook, K., & Driver, S. P. 2008, ArXiv:0804.2892, 804
Bell, E. F., McIntosh, D. H., Katz, N., & Weinberg, M. D. 2003, ApJS, 149, 289
Berlind, A. A. & Weinberg, D. H. 2002, ApJ, 575, 587
Berrier, J. C., Bullock, J. S., Barton, E. J., Guenther, H. D., Zentner, A. R., & Wechsler, R. H. 2006, ApJ, 652, 56
Birnboim, Y., Dekel, A., & Neistein, E. 2007, MNRAS, 380, 339
Borch, A., Meisenheimer, K., Bell, E. F., Rix, H.-W., Wolf, C., Dye, S., Kleinheinrich, M., Kovacs, Z., & Wisotzki, L. 2006, A&A, 453, 869
Bower, R. G., Benson, A. J., Malbon, R., Helly, J. C., Frenk, C. S., Baugh, C. M., Cole, S., & Lacey, C. G. 2006, MNRAS, 370, 645
Brinchmann, J., Charlot, S., White, S. D. M., Tremonti, C., Kauffmann, G., Heckman, T., & Brinkmann, J. 2004, MNRAS, 351, 1151
Brinchmann, J. & Ellis, R. S. 2000, ApJ, 536, L77
Brown, M. J. I., Dey, A., Jannuzi, B. T., Brand, K., Benson, A. J., Brodwin, M., Croton, D. J., & Eisenhardt, P. R. 2007, ApJ, 654, 858
Brown, M. J. I. et al. 2008, arXiv:0804.2293, 804
Bruzual, G. & Charlot, S. 2003, MNRAS, 344, 1000
Bryan, G. L. & Norman, M. L. 1998, ApJ, 495, 80
Bullock, J. S., Wechsler, R. H., & Somerville, R. S. 2002, MNRAS, 329, 246
Bullock, J. S. et al. 2001, MNRAS, 321, 559
Bundy, K., Ellis, R. S., & Conselice, C. J. 2005, ApJ, 625, 621
Cattaneo, A., Dekel, A., Faber, S. M., & Guiderdoni, B. 2008, arXiv:0801.1673, 801
Cattaneo, A. et al. 2007, MNRAS, 377, 63
Cen, R. & Ostriker, J. 1992, ApJ, 393, 22
Chabrier, G. 2003, PASP, 115, 763
Cimatti, A., Daddi, E., & Renzini, A. 2006, A&A, 453, L29
Coil, A. L., Newman, J. A., Cooper, M. C., Davis, M., Faber, S. M., Koo, D. C., & Willmer, C. N. A. 2006, ApJ, 644, 671
Cole, S., Lacey, C. G., Baugh, C. M., & Frenk, C. S. 2000, MNRAS, 319, 168
Cole, S. et al. 2001, MNRAS, 326, 255
Conroy, C., Ho, S., & White, M. 2007a, MNRAS, 379, 1491
Conroy, C. & Ostriker, J. P. 2007, ArXiv:0712.0824, 712
Conroy, C., Shapley, A. E., Tinker, J. L., Santos, M. R., & Lemson, G. 2008, arXiv:0711.0001, 711
Conroy, C., Wechsler, R. H., & Kravtsov, A. V. 2006, ApJ, 647, 201
—. 2007b, ApJ, 668, 826
Conroy, C. et al. 2007c, ApJ, 654, 153
Cool, R. J. et al. 2008, ArXiv:0804.4516
Cowie, L. L., Songaila, A., Hu, E. M., & Cohen, J. G. 1996, AJ, 112, 839
Croton, D. J. et al. 2006, MNRAS, 365, 11
Davé, R. 2008, MNRAS, 385, 147
Dekel, A. & Birnboim, Y. 2006, MNRAS, 368, 2
—. 2008, MNRAS, 383, 119
Drory, N. & Alvarez, M. 2008, ArXiv:0803.1489, 803
Drory, N., Bender, R., Feulner, G., Hopp, U., Maraston, C., Snigula, J., & Hill, G. J. 2004, ApJ, 608, 742
Drory, N., Salvato, M., Gabasch, A., Bender, R., Hopp, U., Feulner, G., & Pannella, M. 2005, ApJ, 619, L131
Fontana, A. et al. 2004, A&A, 424, 23
—. 2006, A&A, 459, 745
Gao, L., White, S. D. M., Jenkins, A., Stoehr, F., & Springel, V. 2004, MNRAS, 355, 819
Gonzalez, A. H., Zabludoff, A. I., & Zaritsky, D. 2005, ApJ, 618, 195
Guo, Q. & White, S. D. M. 2008, MNRAS, 384, 2
Hansen, S. M., Sheldon, E. S., Wechsler, R. H., & Koester, B. P. 2007, ArXiv:0710.3780, 710

Hatton, S., Devriendt, J. E. G., Ninin, S., Bouchet, F. R., Guiderdoni, B., & Vibert, D. 2003, MNRAS, 343, 75
Heavens, A., Panter, B., Jimenez, R., & Dunlop, J. 2004, Nature, 428, 625
Hopkins, A. M. 2004, ApJ, 615, 209
Hopkins, A. M. & Beacom, J. F. 2006, ApJ, 651, 142
Juneau, S. et al. 2005, ApJ, 619, L135
Katz, N., Weinberg, D. H., & Hernquist, L. 1996, ApJS, 105, 19
Kauffmann, G. et al. 2003, MNRAS, 341, 54
Kereš, D., Katz, N., Weinberg, D. H., & Davé, R. 2005, MNRAS, 363, 2
Khochfar, S. & Ostriker, J. P. 2007, ArXiv:0704.2418, 704
Klypin, A., Zhao, H., & Somerville, R. S. 2002, ApJ, 573, 597
Kravtsov, A. V. et al. 2004, ApJ, 609, 35
Krick, J. E. & Bernstein, R. A. 2007, AJ, 134, 466
Lacey, C. & Cole, S. 1993, MNRAS, 262, 627
Lee, J. C., Kennicutt, R. C., Funes, José G., S. J., Sakai, S., & Akiyama, S. 2007, ApJ, 671, L113
Lee, K.-S., Giavalisco, M., Gnedin, O. Y., Somerville, R. S., Ferguson, H. C., Dickinson, M., & Ouchi, M. 2006, ApJ, 642, 63
Li, C., Kauffmann, G., Jing, Y. P., White, S. D. M., Börner, G., & Cheng, F. Z. 2006, MNRAS, 368, 21
Lin, L. et al. 2008, ArXiv:0802.3004, 802
Lucatello, S., Gratton, R. G., Beers, T. C., & Carretta, E. 2005, ApJ, 625, 833
Madau, P., Diemand, J., & Kuhlen, M. 2008, ArXiv e-prints, 802
Maller, A. H., Katz, N., Kereš, D., Davé, R., & Weinberg, D. H. 2006, ApJ, 647, 763
Mandelbaum, R., Seljak, U., Kauffmann, G., Hirata, C. M., & Brinkmann, J. 2006, MNRAS, 368, 715
Marín, F. A., Wechsler, R. H., Frieman, J. A., & Nichol, R. C. 2008, ApJ, 672, 849
Meneux, B. et al. 2008, A&A, 478, 299
Miller, L. 1986, MNRAS, 220, 713
Mo, H. J. & Fukugita, M. 1996, ApJ, 467, L9
Mo, H. J., Jing, Y. P., & White, S. D. M. 1996, MNRAS, 282, 1096
Monaco, P., Murante, G., Borgani, S., & Fontanot, F. 2006, ApJ, 652, L89
Nagamine, K., Ostriker, J. P., Fukugita, M., & Cen, R. 2006, ApJ, 653, 881
Navarro, J. F., Frenk, C. S., & White, S. D. M. 1997, ApJ, 490, 493
Neistein, E., van den Bosch, F. C., & Dekel, A. 2006, MNRAS, 372, 933
Noeske, K. G. et al. 2007a, ApJ, 660, L47
—. 2007b, ApJ, 660, L43
Ostriker, J. P. & Hausman, M. A. 1977, ApJ, 217, L125
Ouchi, M. et al. 2005, ApJ, 635, L117
Panter, B., Jimenez, R., Heavens, A. F., & Charlot, S. 2007, MNRAS, 488
Pérez-González, P. G. et al. 2008, ApJ, 675, 234
Purcell, C. W., Bullock, J. S., & Zentner, A. R. 2007, ApJ, 666, 20
Quadri, R. et al. 2007, ApJ, 654, 138
Reed, D., Governato, F., Quinn, T., Gardner, J., Stadel, J., & Lake, G. 2005, MNRAS, 359, 1537
Reed, D. S., Bower, R., Frenk, C. S., Jenkins, A., & Theuns, T. 2007, MNRAS, 374, 2
Renzini, A. & Ciotti, L. 1993, ApJ, 416, L49
Rich, R. M. et al. 2005, ApJ, 619, L107
Salim, S. et al. 2007, ApJS, 173, 267
Sanderson, A. J. R., Ponman, T. J., & O'Sullivan, E. 2006, MNRAS, 372, 1496
Schiminovich, D. et al. 2007, ApJS, 173, 315
Scoccimarro, R., Sheth, R. K., Hui, L., & Jain, B. 2001, ApJ, 546, 20
Somerville, R. S. & Primack, J. R. 1999, MNRAS, 310, 1087
Spergel, D. N. et al. 2007, ApJS, 170, 377
Springel, V. & Hernquist, L. 2003, MNRAS, 339, 289
Springel, V., White, S. D. M., Tormen, G., & Kauffmann, G. 2001, MNRAS, 328, 726
Steidel, C. C., Adelberger, K. L., Dickinson, M., Giavalisco, M., Pettini, M., & Kellogg, M. 1998, ApJ, 492, 428
Stewart, K. R., Bullock, J. S., Wechsler, R. H., Maller, A. H., & Zentner, A. R. 2007, arXiv:0711.5027, 711
Tasitsiomi, A., Kravtsov, A. V., Wechsler, R. H., & Primack, J. R. 2004, ApJ, 614, 533
Tasitsiomi, A., Wechsler, R. H., Kravtsov, A. V., & Klypin, A. 2008, in preparation
Thomas, D., Maraston, C., Bender, R., & Mendes de Oliveira, C. 2005, ApJ, 621, 673
Tumlinson, J. 2007a, ApJ, 665, 1361
—. 2007b, ApJ, 664, L63
Vale, A. & Ostriker, J. P. 2004, MNRAS, 353, 189
—. 2006, MNRAS, 371, 1173
van den Bosch, F. C. et al. 2007, MNRAS, 376, 841
van Dokkum, P. G. 2008, ApJ, 674, 29
van Zee, L. 2001, AJ, 121, 2003
Wake, D. A. et al. 2006, MNRAS, 372, 537
Wang, L., Li, C., Kauffmann, G., & de Lucia, G. 2006, MNRAS, 371, 537
Wang, P. & Abel, T. 2008, ApJ, 672, 752
Warren, M. S., Abazajian, K., Holz, D. E., & Teodoro, L. 2006, ApJ, 646, 881
Wechsler, R. H., Bullock, J. S., Primack, J. R., Kravtsov, A. V., & Dekel, A. 2002, ApJ, 568, 52
Wechsler, R. H., Gross, M. A. K., Primack, J. R., Blumenthal, G. R., & Dekel, A. 1998, ApJ, 506, 19
Wechsler, R. H., Zentner, A. R., Bullock, J. S., Kravtsov, A. V., & Allgood, B. 2006, ApJ, 652, 71
Wechsler, R. H. et al. 2008, in preparation
White, M., Zheng, Z., Brown, M. J. I., Dey, A., & Jannuzi, B. T. 2007, ApJ, 655, L69
White, S. D. M. & Frenk, C. S. 1991, ApJ, 379, 52
Wilkins, S. M., Trentham, N., & Hopkins, A. M. 2008, MNRAS, 385, 687
Zakamska, N. L. & Narayan, R. 2003, ApJ, 582, 162
Zehavi, I. et al. 2004, ApJ, 608, 16
—. 2005, ApJ, 630, 1
Zentner, A. R., Berlind, A. A., Bullock, J. S., Kravtsov, A. V., & Wechsler, R. H. 2005, ApJ, 624, 505
Zheng, X. Z., Bell, E. F., Papovich, C., Wolf, C., Meisenheimer, K., Rix, H.-W., Rieke, G. H., & Somerville, R. 2007a, ApJ, 661, L41
Zheng, Z., Coil, A. L., & Zehavi, I. 2007b, ApJ, 667, 760
Zibetti, S., White, S. D. M., Schneider, D. P., & Brinkmann, J. 2005, MNRAS, 358, 949